Zircon grain-shape holds provenance information; a case study from southwestern Australia

Makuluni, P.[1], Kirkland, C.L. [*1], Barham, M. [1]

[1]School of Earth and Planetary Sciences, (TIGeR, Centre for Exploration Targeting - Curtin Node), Curtin University, Perth, WA, 6102, Australia
* corresponding author c.kirkland@curtin.edu.au

ABSTRACT

Detrital zircon geochronology is a powerful tool to address a range of geological questions related to sedimentary provenance. Nonetheless, non-unique answers may result when igneous rocks of the same age are sourced from disparate locations. In an effort to resolve some of this issue in zircon provenance investigations, we explore the potential of detrital zircon grains to be linked to their original magmatic source through their grain shape. In order to develop this grain shape measure as a provenance tool we first examine the relationships between chemistry and a range of different grain shape descriptors. We find grain shape to show a linear relationship to U-concentration on a lithologic unit level. We interpret this relationship to be a function of crystal chemical control in igneous samples. Principal component analysis demonstrates the potential of simple grain shape descriptors (major axis, minor axis and effective diameter) to characterise grains from particular rock units. Applying these same shape measures to sedimentary basins in the Proterozoic Albany-Fraser Orogen, in southwest Australia allows us to closely replicate the findings of previous traditional U-Pb geochronological investigations in terms of grain provenance. In addition, we apply this technique to Mesozoic sediment on the southern margin of Australia and show for the first time that its detritus is more likely derived from the underlying crystalline basement rather than surrounding orogens that share similar magmatic ages.

KEYWORDS

Zircon, provenance, Albany-Fraser Orogen, grain shape, statistics, Arid Basin, Barren Basin

INTRODUCTION

Detrital zircon U-Pb geochronology has become a standard technique in reconstructing sediment source and routing, as well as constraining regional tectonomagmatic and depocentre evolutionary histories. Sedimentary provenance investigations through U-Pb geochronology involve determining similarities in the age spectra of detrital zircon populations with those from magmatic and metamorphic zircon crystals in potential source regions. Such U-Pb age similarities can then be utilized to interpret paleogeographic relationships, paleotectonic settings, or test stratigraphic correlations (e.g. Dickinson, 2008, Fedo et al., 2003, Gehrels, 2014). Although detrital zircon U-Pb geochronology has proven effective in tracking source to sink mineral relationships (e.g. Fielding et al., 2017, MacDonald et al., 2013, Xu et al., 2016), in some cases non-unique geological solutions result as zircon growth events may not exclusively correspond to crust-forming events within one source region, thereby limiting the effectiveness of this approach in provenance investigation (Howard et al., 2009). Additional elemental or isotopic information from the same detrital zircon grains, such as Lu-Hf, can provide information on the crustal evolution of source regions, which may be more distinctive and thereby help to overcome some limitations of grain crystallization ages that are not specific to a single source (Lancaster et al., 2011).

In this work, we explore the potential of zircon grain shapes to provide an additional constraint on sediment provenance. We examine the possibility that provenance information can be retained in the morphological characteristics of zircon from its igneous source region to its depositional sink. Zircon grains are highly resistant to both

physical and chemical alteration processes and it has been proposed that they are capable of retaining shape features after going through multiple sedimentary cycles (Baxter, 1977, Dinis and Soares, 2007, Garzanti et al., 2015, Guedes et al., 2011, Markwitz and Kirkland, 2017).

In an effort to expand the utility of the detrital zircon approach in provenance investigations we demonstrate that zircon grain shapes can be used to track grains from their source region to their sink in our case study area and hence provide a further tool in provenance characterization. We aim to identify zircon grain shape descriptors that retain defining signatures of the source rocks and then utilize these same shape descriptors to fingerprint sediment sources for the Barren and Arid Basins of the Albany-Fraser Orogen (AFO) in southwest Western Australia. To achieve this, we first identify grain shape features that may have a relationship with crystallization age or chemistry. Secondly, we utilize selected grain shape features to constrain the provenance of the Barren and Arid Basins, the two major Proterozoic sedimentary successions in this orogen, by establishing a shape link between detrital and magmatic zircon grains. We choose this case study region as the provenance of the Barren and Arid Basins has already been established with a high degree of confidence using both U-Pb geochronology and Lu-Hf isotopic signatures of sediments and source igneous units (Spaggiari et al., 2015). Furthermore, we demonstrate the application of this style of analysis in constraining and refining source regions for Cretaceous sediment on the southern margin of Australia, a region of world-class heavy mineral sand deposits.

BACKGROUND

The morphology of zircon has previously been investigated in a range of studies (Benisek and Finger, 1993, Corfu et al., 2003, Pupin, 1980). There are two major controls on detrital zircon grain shape; the original magmatic or metamorphic

environment where the crystal grew, and the sedimentary transport system that subsequently modified it. Pupin (1980) suggested that water content, chemical composition and temperature of crystallization control the crystal form of magmatic zircon grains and that the relative sizes of zircon prisms {100} and {110} are controlled by crystallization temperature. Vavra (1990) proposed that growth rates and relative sizes of zircon crystal faces are controlled by $ZrSiO_4$ supersaturation and the concentration of other trace elements, rather than temperature. Furthermore, Vavra (1990) observed that the growth of the {110} face is most sensitive to $ZrSiO_4$ supersaturation and concluded that trace element concentration and $ZrSiO_4$ saturation control the morphology of zircon pyramids and prisms respectively. Benisek and Finger (1993) analysed electron microscope images of magmatic zircon crystals oriented perpendicular to their c-axis and concluded that magmatic uranium concentration (U substituting for Zr) strongly controls the prism morphology by producing a growth blocking effect for {110} faces. They also suggested that other chemical substitutions such as Zr^{4+} and Si^{4+} by $Y(REE)^{3+}$ and P^{5+} control zircon prism shapes. Corfu et al. (2003) suggested that the morphology of magmatic zircon grains is strongly controlled by the rate of magma crystallization, ranging from rapidly crystallized acicular crystals to slowly cooled stubby and equant zircon grains.

Fragmentation, mechanical abrasion and dissolution during sedimentary transport reduces grain sizes and definition of original crystal faces through grain fracturing and rounding of grain terminations (Balan et al., 2001, Morton and Hallsworth, 1999). However, zircon grains are generally remarkably mechanically robust and chemically stable when free of significant radiation damage (e.g. Chakoumakos et al., 1987, Guedes et al., 2011; Markwitz et al., 2017). Markwitz and Kirkland (2017) showed that the minor axes of detrital zircon grains were less affected by sedimentary transportation

than the grains major axes and concluded that the minor axis of zircon grains retained a similar character to the magmatic source region better than other grain shape measurements.

GEOLOGICAL SETTING

The Paleo-to-Mesoproterozoic AFO formed during compressional and extensional processes that reworked the southern and south-eastern margins of the Archean Yilgarn Craton (Fig. 1; Spaggiari et al., 2015). The ca. 1815–1600 Ma Barren Basin and the ca. 1455–1305 Ma Arid Basin are regionally extensive sedimentary basins that are incorporated within this orogenic system (Spaggiari et al., 2015, Waddell et al., 2015). Secondary ion mass spectrometry (SIMS) U-Pb zircon geochronology has revealed that the Barren Basin contains Neoarchean zircon detritus whose age and Hf isotopic signatures closely match Archean Yilgarn Craton granites (Kirkland et al., 2011, Kirkland et al., 2015, Smithies et al., 2015, Spaggiari et al., 2015, Wyche et al., 2012). Other enigmatic age components in the Barren Basin cluster around 2250 and 2035 Ma, with Hall et al. (2008) suggesting that they were potentially derived from sources ~1000 km distant in the Gascoyne Province of northwest Western Australia. However, Spaggiari et al. (2015) demonstrated that the detrital zircon Hf isotopic character is distinct from the Gascoyne Province. Common Paleoproterozoic zircon detritus within the Barren Basin share identical age and isotopic signatures to felsic magmatic rocks formed during the 1815–1800 Ma Salmon Gums Event, 1780–1760 Ma Ngadju Event, and 1710–1650 Ma Biranup Orogeny within the AFO (Kirkland et al., 2011, Spaggiari et al., 2015, Spaggiari and Tyler, 2014). The detrital zircon fingerprint of the younger Arid Basin shares a similar Paleoproterozoic component to that of the Barren Basin. However, the Arid Basin lacks significant Archean grains and is dominated by a ca. 1455–1375 Ma detrital zircon age component that is unrecognized in the Barren Basin.

Identical ca. 1400 Ma magmatic zircon ages and Hf isotopic signatures have been identified in the adjacent oceanic Madura Province, specifically from the Haig Cave Supersuite, which lies to the east of the Albany-Fraser Orogen (Kirkland et al., 2017, Spaggiari and Smithies, 2015). Spaggiari et al. (2015) suggested that the Loongana Arc of the Madura Province was accreted at ca. 1330 Ma during closure of the craton marginal Arid Basin (Smithies et al., 2015). The ca. 1400 Ma Haig Cave Supersuite, which is the magmatic expression of the Loongana Arc, is suggested to be the source of the exotic 1455–1375 Ma juvenile detritus within the Arid Basin (Kirkland et al., 2017, Spaggiari et al., 2015).

During later Mesozoic break-up of eastern Gondwana, Cretaceous subsidence associated with rift propagation between Australia and Antarctica, combined with a eustatic high, led to a regional transgression in southern Australia and development of the Madura Shelf of the Bight Basin (Barham et al., in press, Lowry, 1970, Stagg et al., 1990). Madura Shelf sediments variously overly crystalline rocks of the AFO and Madura and Coompana Provinces, as well as older sedimentary basins to the north (Fig. 1; Reynolds, 2016). The Madura and Coompana Provinces appear to have been sourced from a common c. 1950 Ma oceanic crust (Mirning Ocean) that separates the Archean Yilgarn and Gawler Cratons of western and southern Australia respectively (Kirkland et al., 2017). Cretaceous clastics of the Madura Shelf (Loongana and Madura Formations), as well as Cenozoic paleoshoreline sediments are proposed to have been significantly derived from the AFO in southwest Australia and the Musgrave Province in central Australia, with similarities in U-Pb zircon magmatic ages between these regions previously preventing clear distinction in provenance between these sources using geochronology alone (Barham et al., in press, Hou et al., 2011, Reid et al., 2013).

METHODOLOGY AND DESCRIPTIVE STATISTICS

Image processing and data collection

Reflected light images of zircon grains in previously dated samples from several lithotectonic domains of Western Australia, including components of the Albany-Fraser Orogen, Madura Province, southern Yilgarn Craton and Madura Shelf, were used for grain shape analysis (GSWA, 2015, Barham et al., in press). Based on cathodoluminescence images and U-Pb geochronology those grains chosen for shape measurement have minimal to no metamorphic features and hence the measured grains shapes are interpreted to primarily reflect growth during a single event and, in the case of sediments, the additional influence of transportation related modification. Metamorphic features identified in zircon typically constitute homogeneous overgrowths visible in cathodoluminescence images. As metamorphic overgrowths tend to produce an even mantle on zircon cores (Corfu et al., 2003), shape measurements based on ratios will be comparatively unaffected by typical thin metamorphic overgrowths seen in many metasedimentary successions worldwide. In this work we compiled images from 12 sedimentary samples (five from the Arid Basin, four from the Barren Basin and three from the Madura Shelf), and 20 magmatic samples (four from the Esperance Supersuite, two from the Recherche Supersuite, five from Biranup Zone magmatic rocks, all from the AFO, four from the Haig Cave Supersuite, two from Moodini Supersuite, both in the Madura Province, and three from the southern Yilgarn Craton; Supplementary Table 1). Reflected light images were scaled and then processed through a background discrimination routine to isolate grain outlines using ImageJ software (Abramoff et al., 2004). A total of 647 detrital zircon grains (253, 163 and 231 from the Arid, Barren and Bight [Madura Shelf] Basins, respectively) and 412 magmatic zircon grains (64 Esperance Supersuite, 85 Recherche Supersuite, 96

Biranup Zone, 107 Madura Province [87 Haig Cave Supersuite, 20 Moodini Supersuite], and 60 southern Yilgarn Craton) were measured (Supplementary Table 1). For a case of 100 measured grains the fraction that we know with 95% certainty not to have missed is 0.057 (Vermeesch, 2004). A total of nine shape descriptors were measured/calculated to characterize the zircon grains (Table 1). Previously published U-Pb geochronology and uranium and thorium concentrations collected using SIMS (GSWA, 2015) were associated with each grain that had its shape characteristics measured where possible (all samples bar those from the Madura Shelf and the Moodini Supersuite which reflect a test sample set compared using shape characteristics alone; Supplementary Table 1).

Descriptive statistics

Table 2 presents summary statistics of the shape measurements of zircon grains for all the sample regions. Initially we use a Shapiro-Wilk test to explore the distribution of the variables. The null-hypothesis of this test is that the population is normally distributed. Thus, if the p-value is less than 0.05 then the null hypothesis is rejected and there is evidence that the data are not from a normally distributed population. This test establishes that the age variable for all samples shows a more non-parametric distribution than the grain shape measures (effective diameter shown on Fig. 2), which are all closer to, or are, normal distributions. The only exception to this pattern is the Barren Basin population, which clearly has multiple grain shape populations in concert with polymodal age components (Table 2; Spaggiari et al., 2015). The implication of this observation is that although zircon may have grown in different magmatic environments at different times, the grain shape measures for a sample do not, in general, hold the same variability, potentially due to regional crystallization factors that we aim to explore using simple univariate statistical tests before applying more

complex non-parametric analysis. Furthermore, parametric tests (e.g. F and t-tests) can perform well in certain circumstances of non-normal distribution particularly when mean and median are similar, for these reasons we first evaluate differences using some simple statistical tests (Sheskin, 2011).

Statistical tests

GRAIN SHAPE CHARACTERS FOR DISTINGUISHING POPULATIONS

Principal component analysis (PCA) within the statistical software package PAST (Hammer et al., 2001) was used to establish which shape characteristics (obtained from image analysis) are responsible for the greatest dispersion of the measured parameter in order to distinguish unique grain population signatures. Descriptors relating to the magnitude of the 2d axial dimensions of the grain were found to be most significant in distinguishing separate populations, with major axis measurements having the greatest weighting (Fig. 3). Grain perimeter and area also cause strong dispersion on the PC1. Since grain minor length and effective diameter have previously been demonstrated to be faithfully retained through transport processes from their origin (Markwitz et al., 2017), we further explore these characteristics (major axis, minor axis and effective diameter) to assess grain shape as a provenance tool.

CORRELATION OF ZIRCON GRAIN SHAPES WITH U CONTENT

The Pearson Correlation Coefficient was used to evaluate if any linear relationship exists between zircon grain shape parameters and grain chemistry (Table 3). The correlation coefficient value R (between -1 to 1) is the ratio of covariance between the two variables to the product of their standard deviation (Davis, 2002). Thus, the values of R determine the strength of the correlation, with values > 0 indicating a positive relationship of both values increasing in magnitude together and R values less than 0 indicating a negative relationship and the decrease of a variable while the other

increases. Where 0.5> R > -0.5, it is interpreted to indicate a weak correlation, where R < -0.5 or R > 0.5, a moderate to high correlation, and R = 0, no linear correlation between the two variables. Although more complex fits can be made to the data, the purpose of this exercise was to determine if there is any overarching relationship between grain composition and shape (Davis, 2002).

PROVENANCE TESTS USING ZIRCON GRAIN SHAPES: DETRITAL VS IGNEOUS ZIRCON GRAIN SHAPES

Test of equality of variances (F-test)

To evaluate the similarity between selected zircon grain shape features from the sedimentary basins and those from igneous rocks we apply the F-test (Table 4 and 5). The F-test is based on comparing the variances of samples to determine if they are drawn from the same population. The null hypothesis is $\sigma^2_1 = \sigma^2_2$, which states that the two samples are drawn from populations having equal variances (Davis, 2002). The alternative hypothesis states that the variances are not equal; hence we test if a difference is statistically significant by calculating P values with a threshold of ≤ 0.05.

Test of equality of two sample means (two tailed t-test)

We performed t-tests using the appropriate variance model as determined by the F-test (Tables 4 and 5). In the t-test selected detrital zircon grain shape parameter means (major axis, minor axis and effective diameter) were compared against corresponding igneous zircon grain shape parameter means for pooled lithotectonic and basin regions. This statistical test is based upon comparing two sample means to determine if they are similar and hence, whether the samples may be related to the same original zircon population. The null hypothesis, $\mu_1 = \mu_2$, states that the mean of the population from where the sample was drawn is the same as the mean of the parent population (Davis,

2002). The alternative hypothesis, $\mu_1 \neq \mu_2$, indicates the population means are not equal within the specified confidence bounds. This test was performed in Microsoft Excel. Various t-critical values have been calculated (for P = 0.05 and P = 0.01) and presented in Table 4 (Arid and Barren Basins) and Table 5 (Madura Shelf). We take P values >0.05 to indicate strong similarity between the sample means, those between 0.05 and 0.01 to indicate moderate to weak similarity and P values <0.01 to indicate no similarity (Miller and Miller, 2005).

NON-PARAMETRIC (K-S) TEST

More complex statistical tests may be applied to the data set in an effort to extract provenance information. Such non-parametric tests may have greater statistical power given the distribution of grain shape variables. As frequently used in detrital zircon age studies, the Kolmogorov–Smirnov test (K-S test; Vermeesch, 2013) can be utilized to characterize the similarity of grain shape populations. The K-S statistic quantifies the maximum distance (the K-S D value) between the empirical distribution functions of the samples. This distance function can be readily displayed on a multidimensional scaling (MDS) plot (Vermeesch, 2013). MDS is a powerful means of visualizing the level of similarity of samples and is particularly suited to display the information contained in a distance matrix. The application of this technique has been discussed at length with reference to age distributions (Spencer and Kirkland, 2016; Vermeesch, 2013) but is equally as useful to display the relationship between grain shape factors.

RESULTS

Grain shape parameters show some source area distinction based on the mean value of major axis, minor axis and effective diameter. Older Archean zircon crystals from the Yilgarn Craton are on average smaller (effective diameter averaging 83 μm) than younger Mesoproterozoic crystals from the Esperance Supersuite, Recherche

Supersuite and Madura Province (Haig Cave Supersuite), which are relatively larger (effective diameters between 119 and 162 μm; Figure 4 and 5). A similar observation of small Archean Yilgarn zircon grains has previously been made from further north on the craton (Markwitz and Kirkland, 2017).

Correlations of zircon grain shapes with U

Linear regression results from each lithotectonic domain indicate that the zircon major axis is negatively correlated with U concentration in the majority of samples (56%) from crystalline source regions ($p < 0.05$; 67% of samples at $p < 0.1$) (Supplementary Table 2). This crystal shape U correlation may be significant although other potential confounding variables (water content, chemical substitution, $ZrSiO_4$ saturation, temperature of crystallization, modification during grain separation and mounting, etc.) will complicate this relationship. Pooled magmatic suite data show weaker correlations than individual samples likely due to variation in the aforementioned factors (Table 3). The strongest correlation is observed between grain measures and uranium content in the Archean granites of the Yilgarn Craton (Fig. 6). The Barren and Arid Basins data show much more limited correlation of U and shape likely as a combined result of erosive modification of grains and mixing of zircons grown in different environments.

Provenance assessment

SIMILARITY TEST RESULTS: GRAIN SHAPES VS. AGE

Two primary grain shape populations are evident in the Barren Basin samples measured; Mesoproterozoic detrital grains (effective diameter >150 μm), which are most similar to magmatic zircons from the Biranup Zone, and Archean to Paleoproterozoic detrital grains (effective diameter <150 μm) that in part are very similar to magmatic zircons from the Yilgarn Craton (Fig. 4). However, a detrital zircon

subpopulation centred on 2000 Ma does not correspond to any magmatic rocks of the Albany-Fraser Orogen or Yilgarn Craton. Arid Basin detrital grains are all more similar in grain shape than those of the Barren Basin and are most similar in shape to magmatic grains from the Biranup Zone, Madura Province, and Recherche Supersuite (Fig. 4).

VARIANCE (F-TEST) RESULTS

F-test results on major axis and effective diameter indicate no similarity between the Barren Basin and all magmatic sources. However, results using minor axis show strong similarity between Barren Basin samples and those from south Yilgarn Craton and Esperance Supersuite igneous sources. Results using major axis show strong similarity between Arid Basin samples and those from Biranup Zone and Esperance Supersuite. Results using minor axis indicate statistical similarity between Arid Basin and Haig Cave Supersuite, Esperance Supersuite and south Yilgarn Craton. F-tests using effective diameter indicate similarity between Arid Basin and Biranup Zone, Haig Cave Supersuite and Esperance Supersuite.

MEAN (T-TEST) RESULTS

Mean major axis values of detrital zircon grains from the Barren Basin show strong similarity with those of granitic zircons from the Yilgarn Granites (P=0.09) and a moderate correlation with the Haig Cave Supersuite (Supplementary Table 3; Table 4). Similarly, results from the t-test of mean minor axis length demonstrate strong similarity between Barren Basin and Yilgarn Craton zircons with mean minor axis values of 76 µm and 79 µm respectively. On the other hand, results from the t-test of zircon minor axis show no similarity between Barren Basin and the rest of the magmatic samples (Table 4). T-tests using effective diameter shows no similarity between Barren Basin zircons and Yilgarn Craton samples, however it indicates some similarity

between the Barren Basin and Haig Cave Supersuite samples. In summary, the t-test results of major axis and minor axis show statistical similarity between Barren Basin and Yilgarn Craton zircons, and between samples from the Barren Basin and Haig Cave Supersuite (Table 4).

The mean value of the major axis of zircon grains in the Arid Basin is moderately similar to that of grains from the Recherche Supersuite (AFO) and Esperance Supersuite (Table 4). Results from the t-test using zircon grain minor axes indicate strong similarity between Arid Basin detrital zircons and magmatic zircon crystals from the Recherche Supersuite, Haig Cave Supersuite (Madura Province), Biranup Zone and Esperance Supersuite granites. Zircons from the Biranup Zone display the strongest similarity with Arid Basin samples, with mean minor axis values of 120 µm and 118. µm respectively (Supplementary Table 3; Table 4). Results from the t-tests using effective diameter indicates strong similarity between samples from Arid Basin and those from the Recherche Supersuite and Esperance Supersuite and a moderate similarity to the Biranup Zone granites. Overall, t-test results using minor axis, major axis and effective diameter show that shape features of detrital zircons from the Arid Basin display strong statistical similarity to shape features of magmatic zircons from the Biranup Zone granites, Recherche Supersuite and Esperance Supersuite (Table 4).

F-TEST AND T-TEST RESULTS FROM THE TEST SAMPLES OF THE MADURA SHELF

The F-test results are undiagnostic as similarity is shown with many source regions. The t-test shows that the Madura Shelf samples have strong similarity to magmatic zircon grains in the Moodini Supersuite and some similarity to the Haig Cave Supersuite and Yilgarn Craton (Table 5).

NON-PARAMETRIC (K-S TEST) RESULTS

A K-S distance matrix and MDS plot for zircon grain effective diameter is shown in Table 6 and Figure 7 respectively. The non-metric MDS plot is constructed using the Gower distance between K-S D values in 3-D space. The Gower distance is a measure that averages the difference over all variables, each term normalized for the range of that variable and this term appears more effective than Euclidean distance in distinguishing groups (Borg and Groenen, 2005). The MDS plot separates the samples into three distinct fields: Field one, consists of the Yilgarn Granites and the detrital zircon of the Barren Basin. Field two, consists of the magmatic samples from the Esperance and Recherche Supersuites, the granites of the Biranup Zone, and also the detrital grains of the Arid Basin. Field three, consists of the Madura detrital grains and the Moodini and Haig Cave magmatic crystals. A very similar grouping can also be achieved by using a hierarchical clustering routine, on the effective diameter KS-D values, to produce a dendrogram (Borg and Groenen, 2005). Clusters are joined based on the average distance between all members in the two groups (Fig. 7).

Discussion

Correlation of grain shapes with U

Linear regression and correlation coefficient tests indicate that for some regions uranium content can negatively correlate with grain shape (Table 3). Among these three shape descriptors, major axis length shows the strongest negative correlation with U content, followed closely by minor axis. The negative correlation between shape feature (e.g. minor axis) and U content agrees with the conclusions of Benisek and Finger (1993), who proposed that U, which usually substitutes for Zr in the mineral zircon, produces a growth blocking effect on the {110} crystal prism. For prismatic zircon grains, it is likely that sections perpendicular to the c-axis represent the minor axes of

the crystal. Consequently, the growth blocking feature on the {110} prism may affect the minor axis of the zircon grains.

From the Pupin classification chart of zircon morphology and habit (Pupin and Turco, 1972), we propose that the major axis of zircon grains depends on the development of pyramids, i.e. {211}. Our linear regression results (negative correlation of U with either major axis or effective diameter) concur with Vavra (1990), who proposed that the growth of pyramid {211} is controlled by the concentration of trace elements. The negative correlation of zircon major axis lengths with U concentrations (Table 3) suggests that U is among the elements that affect growth of the pyramidal faces {211} on zircon. The zircon structure is made up of chains of alternating edge sharing SiO_4 tetrahedra and ZrO_8 dodecahedra, with oxygen atoms coordinated to Si and Zr at different interatomic distances and angles (Robinson et al., 1971). We propose that, if U replaces Zr in the zircon structure, the interatomic distances and angles are more likely to change due to differences in charge and/or density between Zr and U cations, in accordance with Pauling's rules for substituting elements (Pauling, 1960). This substitution may affect the growth of the pyramid, thereby affecting the major axis and effective diameter characteristics of zircon. This crystal chemistry explanation may also apply to the negative correlation of zircon crystal minor axis length with U concentration. High concentrations of U in magmatic crystals are usually associated with crystal damage and metamict grains that are more susceptible to break-down and removal from the detrital record (Markwitz and Kirkland, 2017). Given the fact that both magmatic and detrital zircon grain populations have both been shown to have a similar relationship between decreasing grain length and increasing U content (Markwitz and Kirkland, 2017), an alternative explanation that high U content leads to greater metamictization and hence reduction in grain size is not favored.

Provenance of Barren and Arid Basins using shape descriptors

Given the strong statistical similarity between Barren Basin zircon grain shape (major axis and minor axis) and southern Yilgarn Craton granites, we suggest that a significant detrital zircon component within the Barren Basin was derived from the southern Yilgarn Craton. Neoarchean zircon crystallization ages (2750-2600 Ma) for granites of the Eastern Goldfields Superterrane of the Yilgarn Craton (Fig. 1) are similar to the ages of a detrital zircon component within the Barren Basin. This Archean detrital zircon age range is dominant in the Lindsay Hill Formation and Stirling Range Formation (Rasmussen et al., 2002) of the AFO, whose proximity and contact relationships with the Yilgarn Craton supports the suggestion that the Yilgarn Craton is a probable source of these sediments in the Barren Basin (Spaggiari et al., 2014). The Barren Basin also contains a significant 2550 Ma to 1900 Ma component; however, this has been interpreted to be sourced from regions distal from the Albany Fraser Orogen (Rasmussen et al., 2002), which cannot be resolved by the currently available grain-shape data.

Results from t-tests also demonstrate moderate statistical similarity between Barren Basin detrital zircon shapes (effective diameter and major axes) and magmatic zircon shapes in Haig Cave granites. However, no correlation is apparent between the Barren Basin and Haig Cave Supersuite on the basis of detrital zircon ages. This result highlights a clear limitation in simplistic correlation tests (e.g. F-and t-tests) that may yield spurious results. Nonetheless, more robust correlations consistent with geochronology are clearer after cluster analysis distinction of discrete subpopulations within the Barren Basin based on their shape characteristics (Fig. 8).

T-test results suggest that Arid Basin zircon samples have strong statistical similarity in terms of their grain shapes to the Recherche and Esperance Supersuites and moderate

similarity with the Biranup Zone granites. The second prominent peak in the age spectrum of detrital zircons in the Arid Basin ranges from 1700 to 1650 Ma and correlates with magmatic crystallization ages of rocks produced in the Biranup Orogeny (Snowys Dam Formation and Gwynn Creek Gneiss; Kirkland et al., 2011, Spaggiari et al., 2014). This correlation is consistent with the similarity in grain shape between zircon crystals in these Biranup magmatic rocks and the detrital grains of the Arid Basin (Fig. 4). Minor axis similarities are consistent with some of the detrital zircon grains in the Arid Basin being sourced from the Haig Cave Supersuite. A dominant detrital zircon age component between 1425 Ma to 1375 Ma is recognised in Arid Basin (meta)sedimentary rocks of the Snowys Dam Formation and Malcom Metamorphics (Spaggiari et al., 2015). Similar ages and Hf isotopic signatures are found within the magmatic rocks of Haig Cave Supersuite of the Madura Province (Kirkland et al., 2017). Although there is grain shape similarity between Arid Basin zircons and the Recherche and Esperance Supersuite, such magmatic zircons cannot be a source given depositional age constraints, again emphasizing the limitations of simplistic statistical correlations.

Similarities in the grain shape characteristics of AFO magmatic zircons (Esperance and Recherche Supersuites and Biranup Zone granites) and Arid Basin detrital zircons sourced from these regions of variable crystallization age, indicate that regional controls on zircon grain shape characteristics may outweigh age specific controls. That is, zircon grains from a specific geographic region may share similarities in their ultimate crystal shapes even though such grains may be derived from temporally disparate magmatic events. The provenance results for detrital zircon grains from the Barren and Arid Basins, using F and t- test on grain shape features, show some correspondence to source-sink patterns determined from zircon U-Pb geochronology.

The MDS plot of effective diameter clearly resolves geologically meaningful source-sink relationships as identified by geochronology. The sedimentary basins all cluster in discrete positions along with their respective dominant magmatic sources. This enables identification of enhanced Yilgarn granite detritus in the Barren Basin and enhanced younger magmatic components in the Arid Basin. Also of note is the regional similarities of igneous rocks, in that Madura Province material all cluster together as do the Proterozoic components of the AFO (Fig. 7). This MDS pattern implies a compositional control on zircon grain shape, likely driven by broad temporal or regional patterns in igneous source composition.

A dendrogram is one method by which grain shape subpopulations can be distinguished within polymodal detrital samples. The grain shape subpopulations corresponded to independently determined discrete age groups demonstrating a remarkable ability to discriminate the number of detrital components represented within a sample. Although some samples may appear normally distributed in terms of a single grain shape parameter, different source regions can still be discerned using cluster analysis techniques extracting information from multiple grain shape descriptors simultaneously (Fig. 8). Hence, we propose that cluster analysis based on grain shape characters should first be undertaken to establish discrete subpopulations that can be tested for provenance relationships on an individual basis through the K-S statistic.

From these results, it is apparent that grain shape descriptors; major axis, minor axis and effective diameter, can be effective in determining the provenance of the Barren and Arid Basin sediments, but clearly cannot be used to place depositional age constraints. Furthermore, these data demonstrate the ability of grain shapes to resolve

the dominant sources from mixed detrital zircon populations that may have the appearance of a single normally distributed zircon population.

Provenance of Madura Shelf zircons

Detrital zircons from the Madura Shelf have been shown to have comparable U/Pb age populations through multiple stratigraphic levels consistent with a stable sediment pool throughout much of the Phanerozoic (from the southerly Officer Basin to Cenozoic paleoshorelines; Barham et al., in press, Reid et al., 2013). Significantly, the paleoshorelines play host to world-class heavy mineral sand deposits that have been upgraded through recycling of this regional stable sediment reservoir (Hou et al., 2011, Reid et al., 2013). Previously, the AFO and Musgrave Province have been implicated as the major source regions for these sediments based on U/Pb geochronology (Barham et al., in press, Hou et al., 2011, Reid et al., 2013). However, similarities in the geological histories of the AFO and Musgrave orogenic systems has made distinguishing zircon routing from them difficult based on geochronology alone. Grain-shape analysis of detrital grains from the Madura Shelf suggest that the AFO was not a major source of zircon to the Madura Shelf (Table 5). However, despite some correlation of zircon grain shape characters with the underlying Haig Cave Supersuite (Table 5), magmatic ages of ca. 1400 Ma are not found in the Madura Shelf sediment (Barham et al., in press) and clearly preclude the Haig Cave Supersuite as a possible source region. Zircon grain shapes reported for the Musgrave Province (Markwitz and Kirkland, 2017) are also significantly different to those measured for the Madura Shelf sediments (mean minor axis of ~75 μm vs 131 μm and mean major axis of ~167 μm vs ~225 μm for the Madura Shelf and Musgrave Province respectively). However, grain shape measurements of magmatic zircons from the ca. 1170 Ma Moodini Supersuite of the Madura Province (samples 192595 and 192565) demonstrate statistically strong

similarities with Madura Shelf zircons minor axis length (~78 μm vs ~75 μm), and major axis length (~178 μm vs ~167 μm), as well as, moderate correlation with effective diameter (~119 μm vs ~110 μm; Supplementary Table 1; Table 5). This suggests that there is a relatively characteristic grain shape for the broader Madura Province (represented by the Haig Cave and Moodini Supersuites). Therefore, we propose zircons of the Madura Shelf, and by inference significant components of the heavy mineral sand deposits regionally, were actually principally derived from the underlying Madura Province basement rather than the AFO or Musgrave Province (Fig. 7).

CONCLUSIONS

Statistical tests on the shapes and chemistry of 1059 zircon grains from 32 samples demonstrate that uranium concentration has an impact on the shape and size of magmatic zircon crystals and that distinctive shape characteristics are preserved through to detrital grains.

High concentrations of U in the Yilgarn Craton granites relate to shorter zircon minor axis, major axis and effective diameter. This negative correlation of U with minor axis may be due to a growth blocking effect that these elements have on prism faces {110}. The negative correlation of U with both major axis and effective diameter may also be due to a similar growth blocking effect but on pyramid faces {211}.

Minor axis, major axis and effective diameter of zircon grains in detrital grains can be used to effectively constrain sediment provenance through non-parametric statistical approaches. However, simple statistical test such as the T-tests are superior to population variance-based F-tests at recognising correlations between detrital and parent magmatic zircon populations. Nonetheless, F-tests may have power in resolving the complexity of source region supply as opposed to correlations between sources and

sinks. For example, in the case of the Madura Shelf the F-test indicates a small degree of grain shape variance in this sediment, similar to that in many magmatic sources. This observation on variance implies the consistent sourcing of the Madura Shelf sediments from a homogeneous age specific source. In contrast the F-test for the Barren Basin shows much greater variance as a result of incorporation of significantly different age and shape populations and hence little variance similarity to sources (Table 4 and 5).

More complex measures of population grain shape similarities involving cluster analysis and KS D values appear to yield more refined provenance results with strong similarity to source – sink relationships established through geochronology. We demonstrate that provenance data are still retrievable from grain shapes in mixed source detrital populations through cluster analysis. Such analysis is capable of defining subpopulations that can refine sediment source inferences.

Using this zircon grain-shape based provenance methodology we propose a revision of the primary sediment sourcing for material on the Madura Shelf. Specifically, we suggest that much of Madura Shelf sediments were sourced directly from their underlying crystalline basement rocks, and suggest that there is a regional characteristic zircon shape for the Madura Province dictated by its geological history, rather than just the magmatic crystallization environment.

These results on zircon grain shape as a provenance tool have significant implications for rapid and low-cost preliminary investigations of sediment provenance generally, and the exploration of heavy mineral sand resources, specifically. Ultimately, zircon grain size and shape play a fundamental role in determining the conditions and processes that mobilise and deposit these grains and therefore influence the depositional settings they will accumulate in.

ACKNOWLEDGEMENTS

Patrick Makuluni would like to thank the University of Malawi for financial support. The authors thank the editor Shane Tyrrell as well as Dave Chew and an anonymous reviewer for constructive comments and reviews that helped improve and clarify the manuscript. The Geological Survey of Western Australia is thanked for making public a wide array of geochronology datasets.

REFERENCES

Abramoff, M., Magalhaes, P. & Ram, S. 2004. Image processing with ImageJ. *Biophotonics International, 11***,** 36-42.

Balan, E., Neuville, D. R., Trocellier, P., Fritsch, E., Muller, J.-P. & Calas, G. 2001. Metamictization and chemical durability of detrital zircon. *American Mineralogist, 86***,** 1025.

Barham, M., Reynolds, S., Kirkland, C. L., O'Leary, M. J., Evans, N. J., Allen, H., Haines, P. W., Hocking, R. M. & McDonald, B. J. in press. Sediment routing and basin evolution in Proterozoic to Mesozoic east Gondwana: a case study from southern Australia. *Gondwana Research*.

Baxter, J. L. 1977. *Heavy mineral sand deposits of Western Australia*, Geological Survey of Western Australia, Mineral Resources Bulletin 10.

Benisek, A. & Finger, F. 1993. Factors controlling the development of prism faces in granite zircons: a microprobe study. *Contributions to Mineralogy and Petrology, 114***,** 441-451.

Borg, I., & Groenen, P. 2005. *Modern Multidimensional Scaling: theory and applications* (2nd ed.). New York: Springer-Verlag. pp. 207–212.

Chakoumakos, B. C., Murakami, T., Lumpkin, G. R. & Ewing, R. C. 1987. Alpha-Decay—Induced Fracturing in Zircon: The Transition from the Crystalline to the Metamict State. *Science, 236***,** 1556-1559.

Corfu, F., Hanchar, J. M., Hoskin, P. W. O. & Kinny, P. 2003. Atlas of Zircon Textures. *Reviews in Mineralogy and Geochemistry, 53***,** 469.

Davis, J. C. 2002. *Statistics and data analysis in Geology*, New York, Wiley.

Dawson, G. C., Krapež, B., Fletcher, I. R., Mcnaughton, N. J. & Rasmussen, B. 2002. Did late Palaeoproterozoic assembly of proto-Australia involve collision between the Pilbara, Yilgarn and Gawler Cratons? Geochronological evidence from the Mount Barren Group in the Albany–Fraser Orogen of Western Australia. *Precambrian Research, 118***,** 195-220.

Dickinson, W. R. 2008. Impact of differential zircon fertility of granitoid basement rocks in North America on age populations of detrital zircons and implications for granite petrogenesis. *Earth and Planetary Science Letters, 275***,** 80-92.

Dinis, P. A. & Soares, A. F. 2007. Stable and ultrastable heavy minerals of alluvial to nearshore marine sediments from Central Portugal: Facies related trends. *Sedimentary Geology, 201***,** 1-20.

Fedo, C. M., Sircombe, K. N. & Rainbird, R. H. 2003. Detrital zircon analysis of the sedimentary record. *Reviews in Mineralogy and Geochemistry, 53***,** 277-303.

Fielding, L., Najman, Y., Millar, I., Butterworth, P., Ando, S., Padoan, M., Barfod, D. & Kneller, B. 2017. A detrital record of the Nile River and its catchment. *Journal of the Geological Society, 174***,** 301-317.

Garzanti, E., Resentini, A., Andò, S., Vezzoli, G., Pereira, A. & Vermeesch, P. 2015. Physical controls on sand composition and relative durability of detrital minerals during ultra-long distance littoral and aeolian transport (Namibia and southern Angola). *Sedimentology, 62***,** 971-996.

Gehrels, G. 2014. Detrital Zircon U-Pb Geochronology Applied to Tectonics. *Annual Review of Earth and Planetary Sciences, 42***,** 127-149.

GSWA 2015. Compilation of geochronology information 2015. *In:* AUSTRALIA, G. S. O. W. (ed.).

Guedes, C. C. F., Giannini, P. C. F., Nascimento, D. R., Sawakuchi, A. O., Tanaka, A. P. B. & Rossi, M. G. 2011. Controls of heavy minerals and grain size in a holocene regressive barrier (Ilha Comprida, southeastern Brazil). *Journal of South American Earth Sciences, 31***,** 110-123.

Hall, C. E., Jones, S. A. & Bodorkos, S. 2008. Sedimentology, structure and SHRIMP zircon provenance of the Woodline Formation, Western Australia: Implications for the tectonic setting of the West Australian Craton during the Paleoproterozoic. *Precambrian Research, 162***,** 577-598.

Hammer, Ø., Harper, D. A. T., & Ryan, P. D. 2001. PAST: Paleontological statistics software package for education and data analysis. *Palaeontologia Electronica, 4*, 1-9.Hartman, P. & Perdok, W. G. 1955. On the relations between structure and morphology of crystals. II. *Acta Crystallographica, 8***,** 521-524.

Hou, B., Keeling, J., Reid, A., Fairclough, M., Wairland, I., Belousova, E., Frakes, L. & Hocking, R. 2011. Heavy mineral sands in the Eucla Basin, Southern Australia: depositional and province-scale prospectivity. *Economic Geology, 106***,** 687-712.

Howard, K. E., Hand, M., Barovich, K. M., Reid, A., Wade, B. P. & Belousova, E. A. 2009. Detrital zircon ages: Improving interpretation via Nd and Hf isotopic data. *Chemical Geology, 262***,** 277-292.

Kirkland, C. L., Smithies, R. H., Spaggiari, C. V., Wingate, M. T. D., Quentin De Gromard, R., Clark, C., Gardiner, N. J. & Belousova, E. A. 2017. Proterozoic crustal evolution of the Eucla basement, Australia: Implications for destruction of oceanic crust during emergence of Nuna. *Lithos, 278–281***,** 427-444.

Kirkland, C. L., Spaggiari, C. V., Pawley, M. J., Wingate, M. T. D., Smithies, R. H., Howard, H. M., Tyler, I. M., Belousova, E. A. & Poujol, M. 2011. On the edge: U–Pb, Lu–Hf, and Sm–Nd data suggests reworking of the Yilgarn craton margin during formation of the Albany-Fraser Orogen. *Precambrian Research, 187***,** 223-247.

Kirkland, C. L., Spaggiari, C. V., Smithies, R. H., Wingate, M. T. D., Belousova, E. A., Gréau, Y., Sweetapple, M. T., Watkins, R., Tessalina, S. & Creaser, R. 2015. The affinity of Archean crust on the Yilgarn—Albany–Fraser Orogen boundary: Implications for gold mineralisation in the Tropicana Zone. *Precambrian Research, 266***,** 260-281.

Lancaster, P. J., Storey, C. D., Hawkesworth, C. J. & Dhuime, B. 2011. Understanding the roles of crustal growth and preservation in the detrital zircon record. *Earth and Planetary Science Letters, 305***,** 405-412.

Lowry, D. C. 1970. Geology of the Western Australian part of the Eucla Basin. *In:* AUSTRALIA, G. S. O. W. (ed.). Perth: Geological Survey of Western Australia.

Macdonald, J. D., Holford, S. P., Green, P. F., Duddy, I. R., King, R. C. & Backé, G. 2013. Detrital zircon data reveal the origin of Australia's largest delta system. *Journal of the Geological Society, 170***,** 3-6.

Markwitz, V. & Kirkland, C. L. 2017. Source to sink zircon grain shape: Constraints on selective preservation and significance for Western Australian Proterozoic basin provenance. *Geoscience Frontiers*.

Miller, J.N., & Miller, J.C. 2010. Statistics and Chemometrics for Analytical Chemistry, Sixth Edition, Pearson, 268p.

Morton, A. C. & Hallsworth, C. R. 1999. Processes controlling the composition of heavy mineral assemblages in sandstones. *Sedimentary Geology, 124***,** 3-29.

Pauling, L. 1960. *The nature of the chemical bond and the structure of molecules and crystals: an introduction to modern structural chemistry*, New York, Cornell University Press.

Pupin, J. P. 1980. Zircon and granite petrology. *Contributions to Mineralogy and Petrology, 73***,** 207-220.

Pupin, J. P. & Turco, G. 1972. Une typologie originale du zircon accessorie. *Bulletin Societe Francais Mineralogie Crystallographie, 95***,** 348-359.

Rasmussen, B., Bengtson, S., Fletcher, I. R. & Mcnaughton, N. J. 2002. Discoidal Impressions and Trace-Like Fossils More Than 1200 Million Years Old. *Science, 296***,** 1112.

Reid, A., Keeling, J., Boyd, D., Belousova, E. & Hou, B. 2013. Source of zircon in world-class heavy mineral placer deposits of the Cenozoic Eucla Basin, southern Australia from LA-ICPMS U–Pb geochronology. *Sedimentary Geology, 286–287***,** 1-19.

Reynolds, S. 2016. Stratigraphic evolution of the southern Australian onshore Bight Basin: a record for the breakup of Gondwana during the Cretaceous. Geological Survey of Western Australia Record 2016/11.

Robinson, K., Gibbs, G. V. & Ribbie, P. H. 1971. The structure of zircon: a comparison with garnet. *The American Mineralogist, 56***,** 782-790.

Russ, J.C. 2011. *The Image Processing Handbook*, Sixth Edition, Florida, CRC Press Inc.

Sheskin, D.J. 2011. Handbook of parametric and nonparametric stratistical procedures, 5th edition. Taylor and Francis, 1926p.

Smithies, R. H., Spaggiari, C. V. & Kirkland, C. L. 2015. *Building the crust of the Albany-Fraser Orogen; constraints from granite geochemistry*, East Perth, W.A, Geological Survey of Western Australia, Report 150.

Spaggiari, C. V., Kirkland, C. L., Smithies, R. H. & Wingate, M. T. D. 2014. Tectonic links between Proterozoic sedimentary cycles, basin formation and magmatism in the Albany–Fraser Orogen. Geological Survey of Western Australia, Report 133.

Spaggiari, C. V., Kirkland, C. L., Smithies, R. H., Wingate, M. T. D. & Belousova, E. A. 2015. Transformation of an Archean craton margin during Proterozoic basin formation and magmatism: The Albany–Fraser Orogen, Western Australia. *Precambrian Research, 266***,** 440-466.

Spaggiari, C. V. & Smithies, R. H. 2015. Eucla basement stratigraphic drilling results release workshop: extended abstracts.

Spaggiari, C. V. & Tyler, I. M. 2014. *Albany-Fraser Orogen seismic and magnetotelluric (MT) workshop 2014: extended abstracts*, Geological Survey of Western Australia Record 2014/6.

Spencer, C. J., and Kirkland, C. L. 2016. Visualizing the sedimentary response through the orogenic cycle: A multidimensional scaling approach. *Lithosphere, 8, n. 1*, 29-37.

Stagg, H. M. J., Cockshell, C. D., Willcox, J. B., Hill, A. J., Needham, D. J. L., Thomas, B., O'brien, G. W. & Hough, L. P. 1990. *Basins of the Great Australian Bight region: geology and petroleum potential*, Bureau of Mineral Resources, Continental Margins Program Folio 5.

Vavra, G. 1990. On the kinematics of zircon growth and its petrogenetic significance: a cathodoluminescence study. *Contributions to Mineralogy and Petrology, 106***,** 90-99.

Vermeesch, P. 2004. How many grains are needed for a provenance study? *Earth and Planetary Science Letters, 224*, n.3-4, 441-451

Vermeesch, P. 2013. Multi-sample comparison of detrital age distributions. *Chemical Geology, 341*, 140-146.

Waddell, P.-J. A., Timms, N. E., Spaggiari, C. V., Kirkland, C. L. & Wingate, M. T. D. 2015. Analysis of the Ragged Basin, Western Australia: Insights into syn-orogenic basin evolution within the Albany–Fraser Orogen. *Precambrian Research, 261***,** 166-187.

Wyche, S., Kirkland, C. L., Riganti, A., Pawley, M. J., Belousova, E. & Wingate, M. T. D. 2012. Isotopic constraints on stratigraphy in the central and eastern Yilgarn Craton, Western Australia. *Australian Journal of Earth Sciences, 59***,** 657-670.

Xu, J., Snedden, J. W., Stockli, D. F., Fulthorpe, C. S. & Galloway, W. E. 2016. Early Miocene continental-scale sediment supply to the Gulf of Mexico Basin based on detrital zircon analysis. *Geological Society of America Bulletin*.

Figure captions

1 - Simplified, interpreted bedrock geology of SW Australia showing the Yilgarn Craton, Albany–Fraser Orogen, Madura Province, and overlying Madura Shelf. The western Nornalup Zone includes Recherche and Esperance Supersuite intrusions that are not distinguished (modified from Spaggiari et al., 2015). Overlaid stipple indicates younger sedimentary sequences. Note that Cenozoic Eucla Basin sediments that cover parts of the SE Albany-Fraser Orogen and the entire Madura Shelf have been omitted. Filled circles denote sample locations.

2 – Bar chart of Shapiro-Wilk P value for normality (effective diameter and age) of zircon grains in geological units of SW Australia.

3 – Bar chart of the principal component loadings for different grain shape parameters in zircons. Black fill denotes shape characteristics utilized in further analyses.

4 – Age ($^{207}Pb/^{206}Pb$) versus specified grain shape parameter (effective diameter, major and minor axis) plots for magmatic and detrital zircons of the Yilgarn Craton, Albany–Fraser Orogen, Madura Province, and Madura Shelf. Inset on right hand margin shows histograms of the shape parameter with a kernel density estimate. Source regions are indicated by triangles whereas sink regions are indicated by circles. MU indicates median zircon grain shape for c. 1200 Ma Musgrave Province magmatic rocks. Mo indicates median zircon grain shape for the Moodini Supersuite of the Madura Province.

5 – Illustrative zircons grains from the principal crystalline sources studied. Simplified crystal outlines represent relatively scaled average zircon dimensions for the respective source populations, with inset numbers representing average minor and major crystal axes in microns. U-Pb geochronology for these samples is published in the Compilation of geochronology information: Geological Survey of Western Australia, http://www.dmp.wa.gov.au/geochron.

6 – Major axis versus U plot with linear regression (dashed line) for zircon grains of the Yilgarn Craton.

7 – a: Multidimensional scaling plot (KS-D values) of zircon effective diameter for source and sink regions coloured according to clusters as defined in part b. b: dendrogram of effective diameter KS-D values. The phenon line (dashed) at a distance value of 0.3 defines three discrete clusters.

8 – Dendrograms distinguishing subpopulations of zircons based on a range of grain shape parameters (as defined in table 2). A phenon line at 3.5 (dashed) defines distinct subpopulations, which are shown with their respective age probability curves (probability density - solid curve, kernel density - dashed curve). Schematic grain shapes are also shown for each subpopulation with mean major and minor axis values stated.

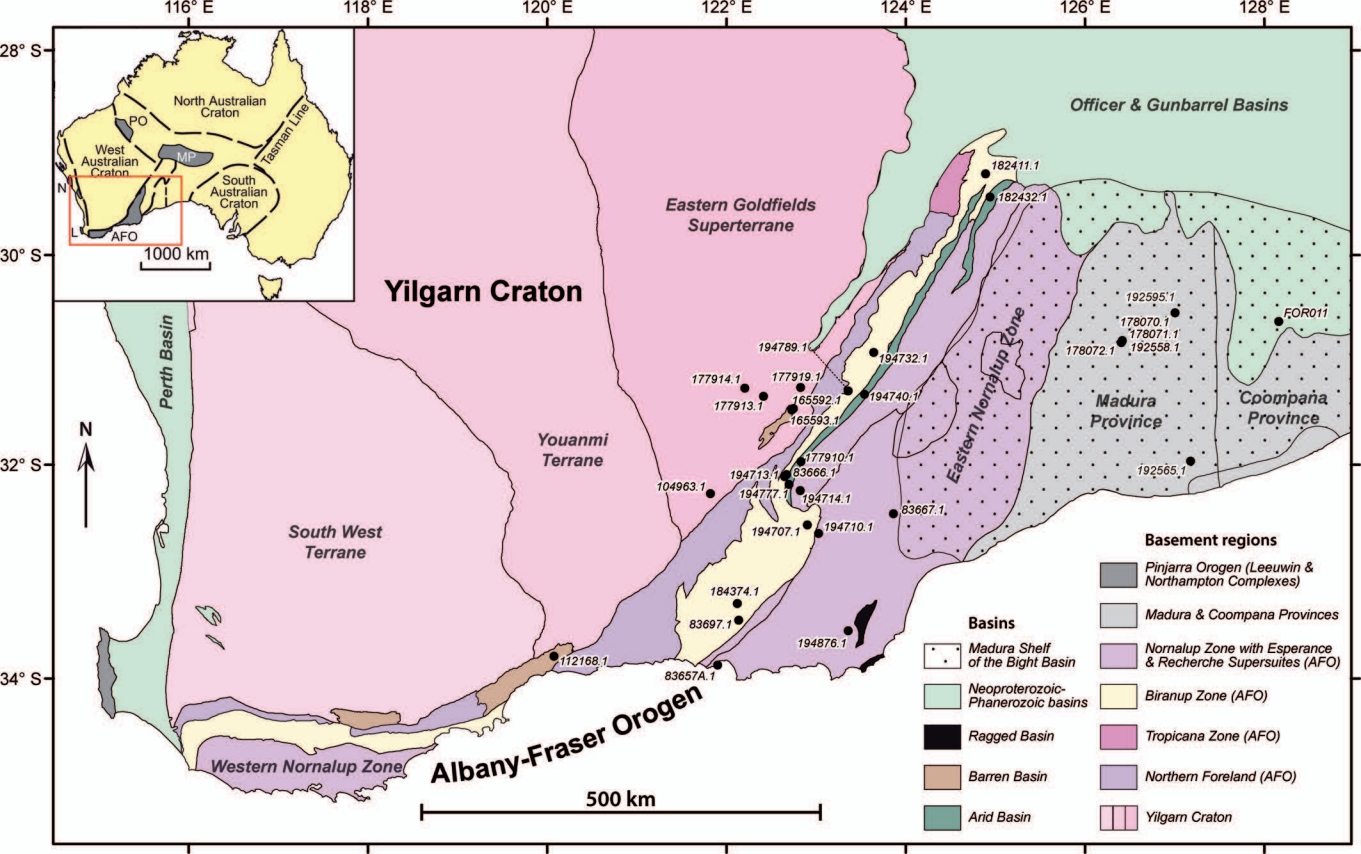
116° E
118° E
120° E
122° E
124° E
126° E
128° E
28° S
30° S
32° S
34° S
North Australian Craton
PO
West Australian Craton
MP
Tasman Line
South Australian Craton
N
L
AFO
1000 km
Yilgarn Craton
Officer & Gunbarrel Basins
Eastern Goldfields Superterrane
Perth Basin
Youanmi Terrane
South West Terrane
Eastern Nornalup Zone
Madura Province
Coompana Province
Western Nornalup Zone
Albany-Fraser Orogen
500 km
N
182411.1
182432.1
192595.1
178070.1
178071.1
178072.1
192558.1
FOR011
194789.1
194732.1
177914.1
177919.1
177913.1
165592.1
194740.1
165593.1
177910.1
83666.1
194713.1
104963.1
194777.1
194714.1
83667.1
194707.1
194710.1
192565.1
184374.1
83697.1
194876.1
112168.1
83657A.1
Basement regions
Pinjarra Orogen (Leeuwin & Northampton Complexes)
Madura & Coompana Provinces
Nornalup Zone with Esperance & Recherche Supersuites (AFO)
Biranup Zone (AFO)
Tropicana Zone (AFO)
Northern Foreland (AFO)
Yilgarn Craton
Basins
Madura Shelf of the Bight Basin
Neoproterozoic-Phanerozoic basins
Ragged Basin
Barren Basin
Arid Basin

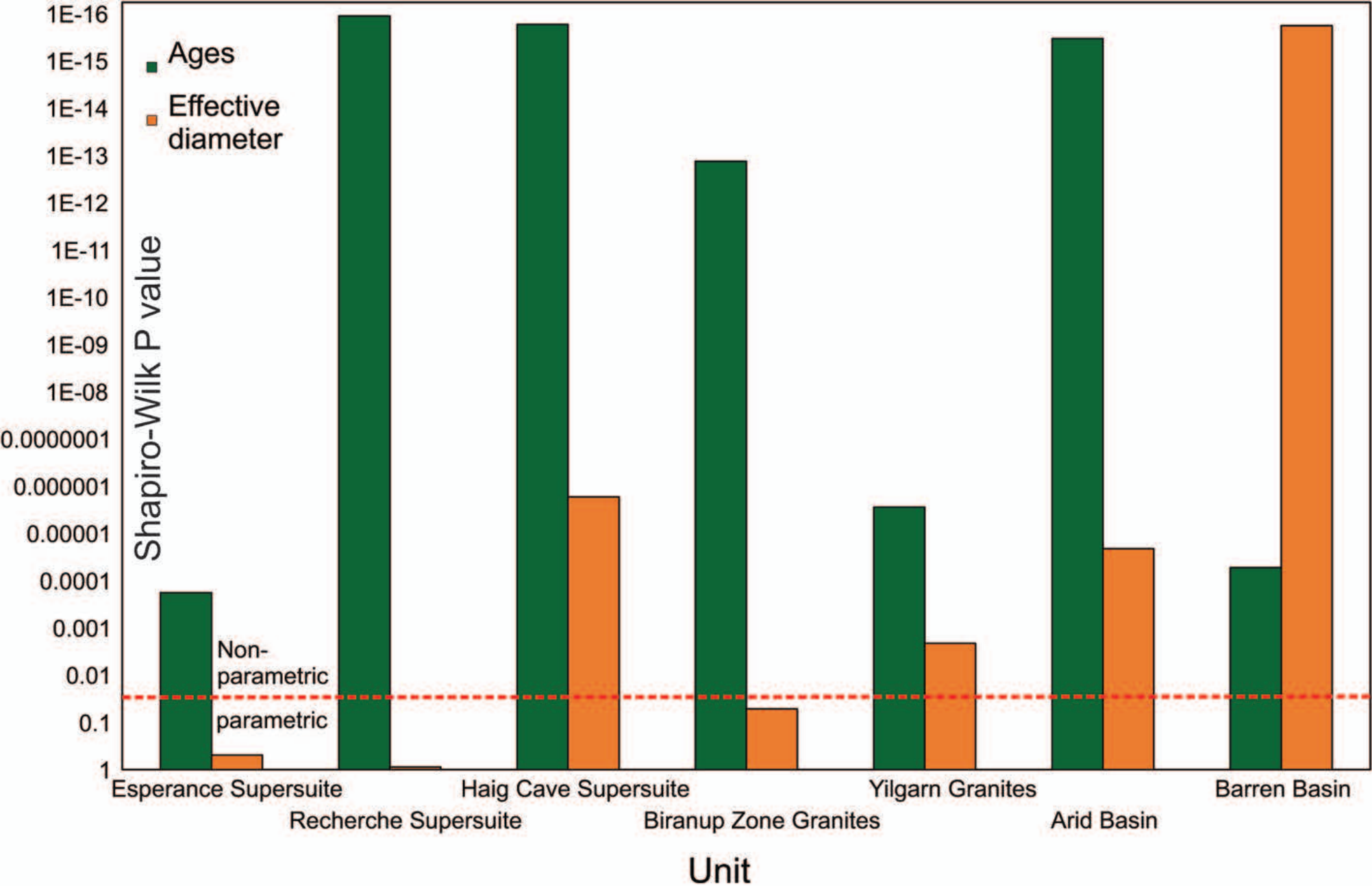
Ages
Effective diameter
Shapiro-Wilk P value
1E-16
1E-15
1E-14
1E-13
1E-12
1E-11
1E-10
1E-09
1E-08
0.0000001
0.000001
0.00001
0.0001
0.001
0.01
0.1
1
Non-parametric
parametric
Esperance Supersuite
Recherche Supersuite
Haig Cave Supersuite
Biranup Zone Granites
Yilgarn Granites
Arid Basin
Barren Basin
Unit

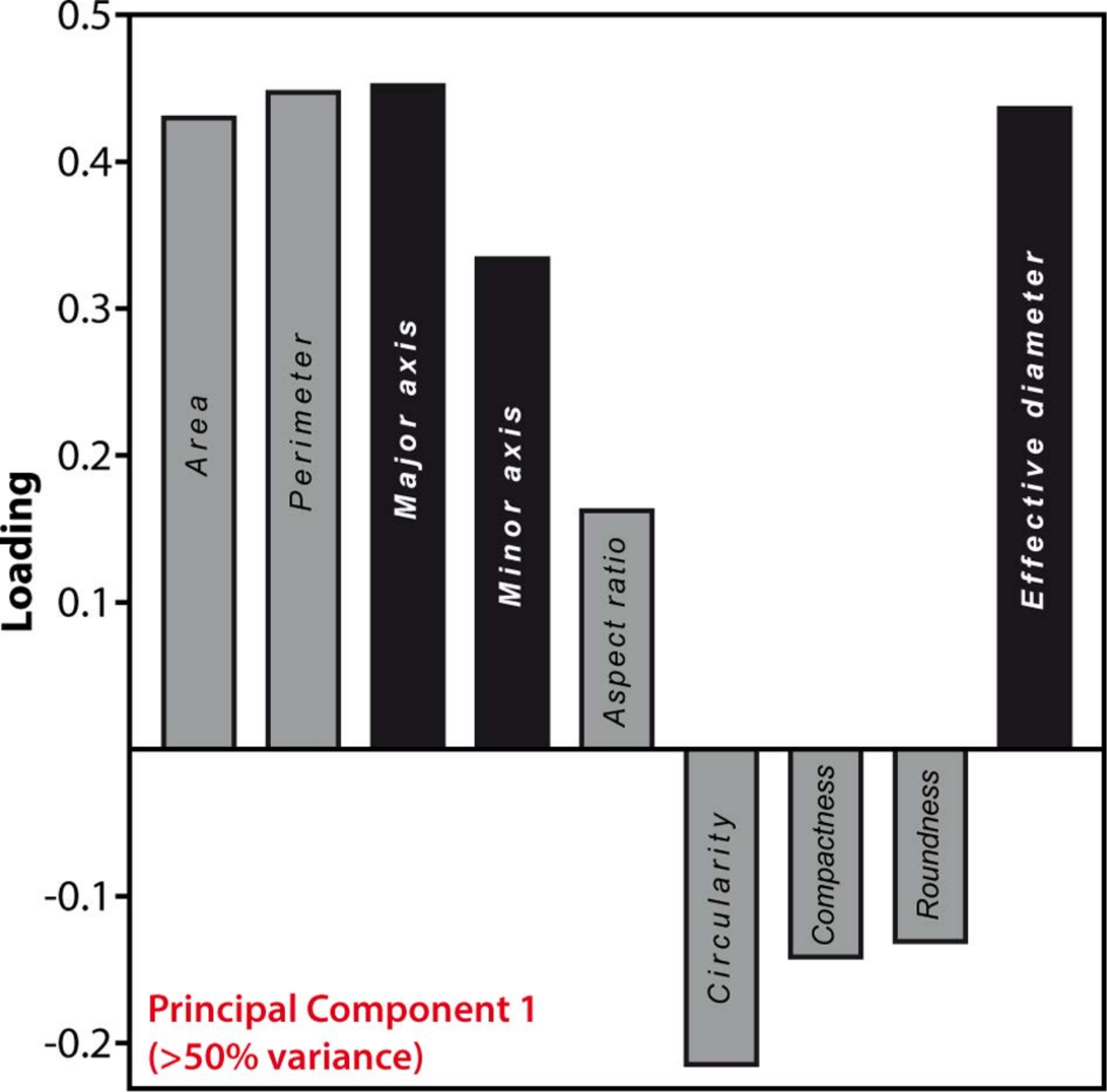
Loading
0.5
0.4
0.3
0.2
0.1
-0.1
-0.2
Area
Perimeter
Major axis
Minor axis
Aspect ratio
Circularity
Compactness
Roundness
Effective diameter
Principal Component 1
(>50% variance)

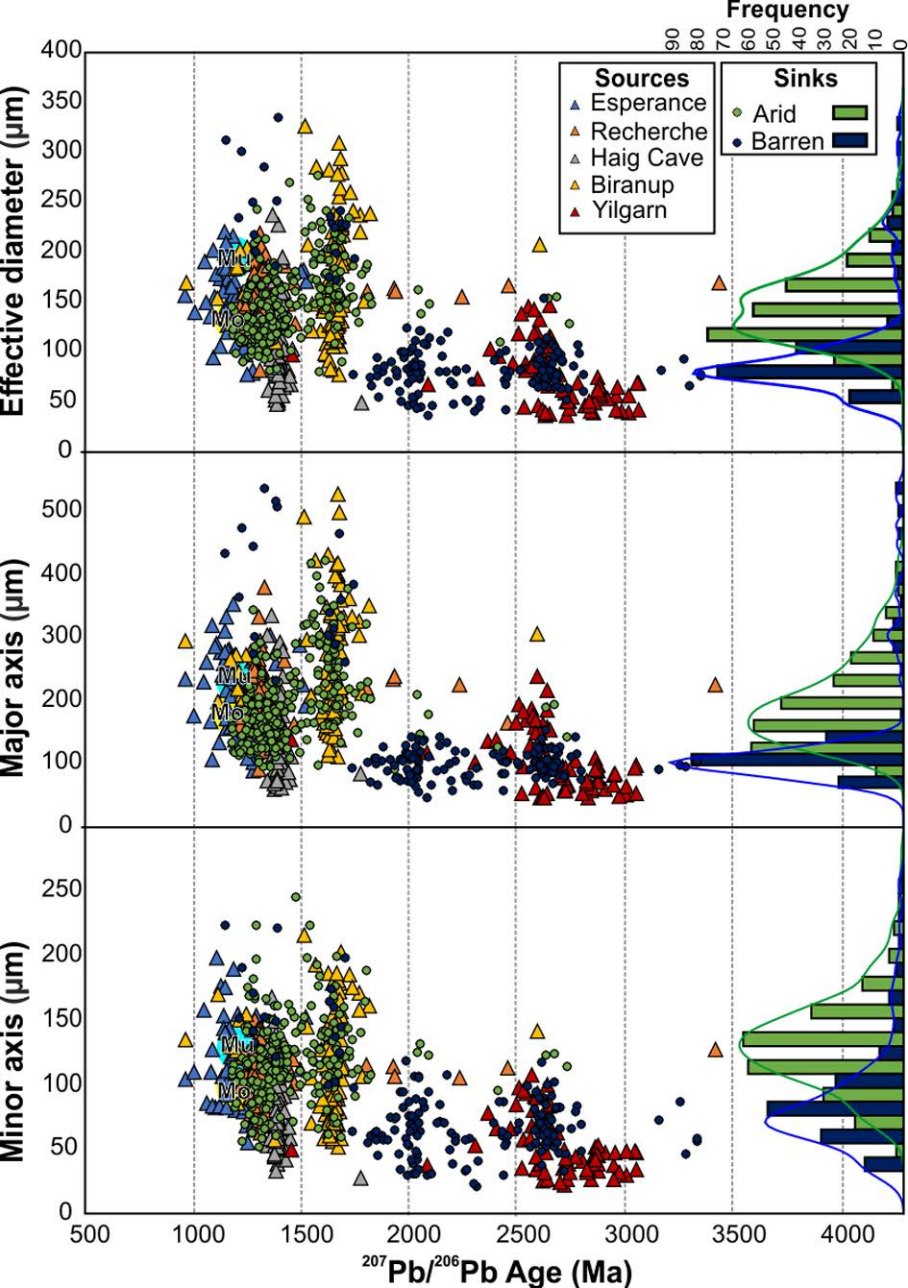
Frequency
90
80
70
60
50
40
30
20
10
0
Sources
Esperance
Recherche
Haig Cave
Biranup
Yilgarn
Sinks
Arid
Barren
Effective diameter (µm)
400
350
300
250
200
150
100
50
0
Mu
Mo
Major axis (µm)
500
400
300
200
100
0
Minor axis (µm)
250
200
150
100
50
0
500
1000
1500
2000
2500
3000
3500
4000
207Pb/206Pb Age (Ma)

79 x 117

Yilgarn Craton 104963_3
^{238}U 749 ppm; 3021 Ma

120 x 218

Biranup Zone
83666_1
^{238}U 386 ppm; 1638 Ma

112 x 152

Haig Cave Supersuite
178072_17
^{238}U 201 ppm; 1407 Ma

114 x 210

Recherche Supersuite
194710_40
^{238}U 109 ppm; 1356 Ma

112 x 215

Esperance Supersuite
83657A_3
^{238}U 305 ppm; 1133 Ma

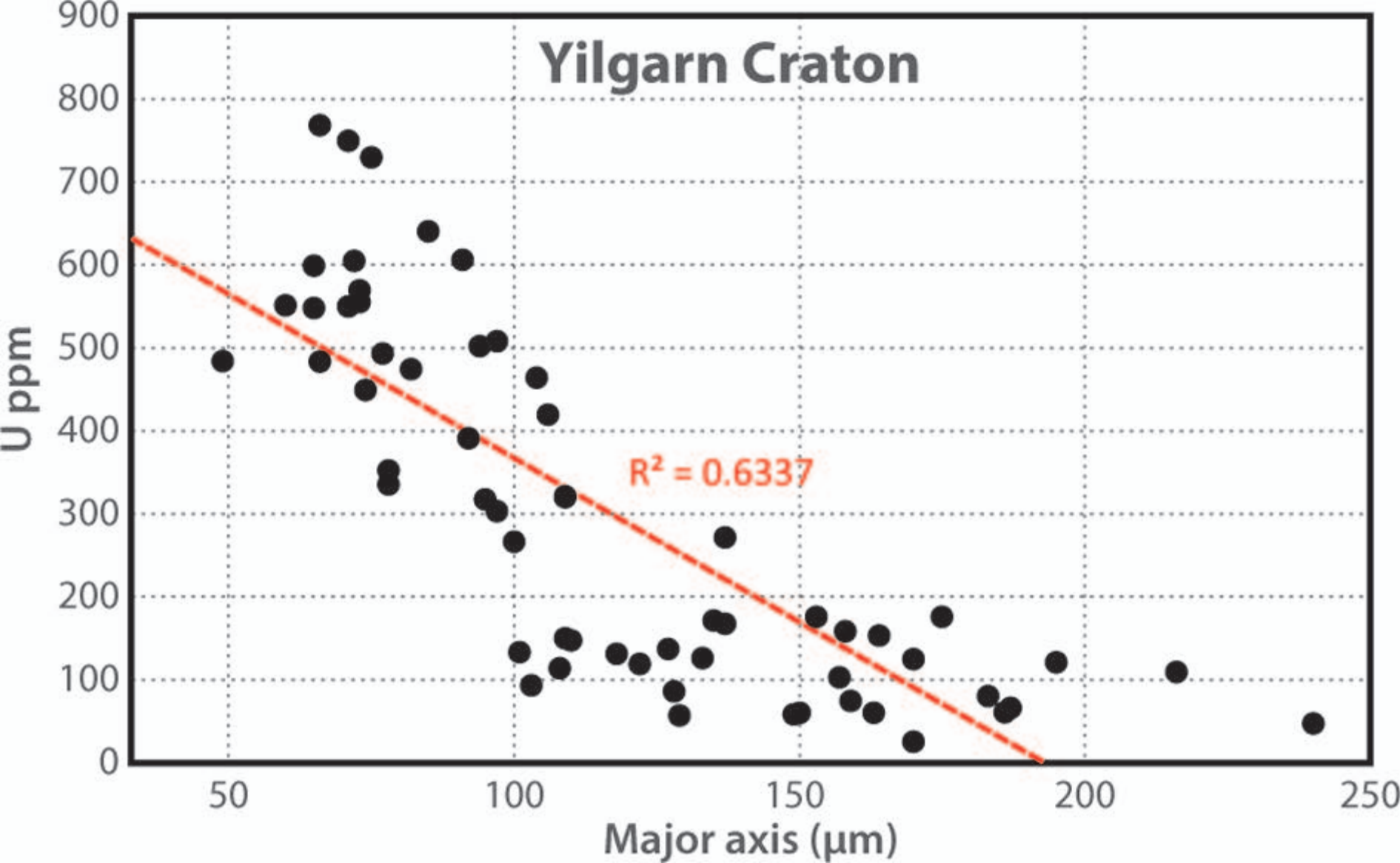
Yilgarn Craton
R² = 0.6337
U ppm
Major axis (µm)
900
800
700
600
500
400
300
200
100
0
50
100
150
200
250

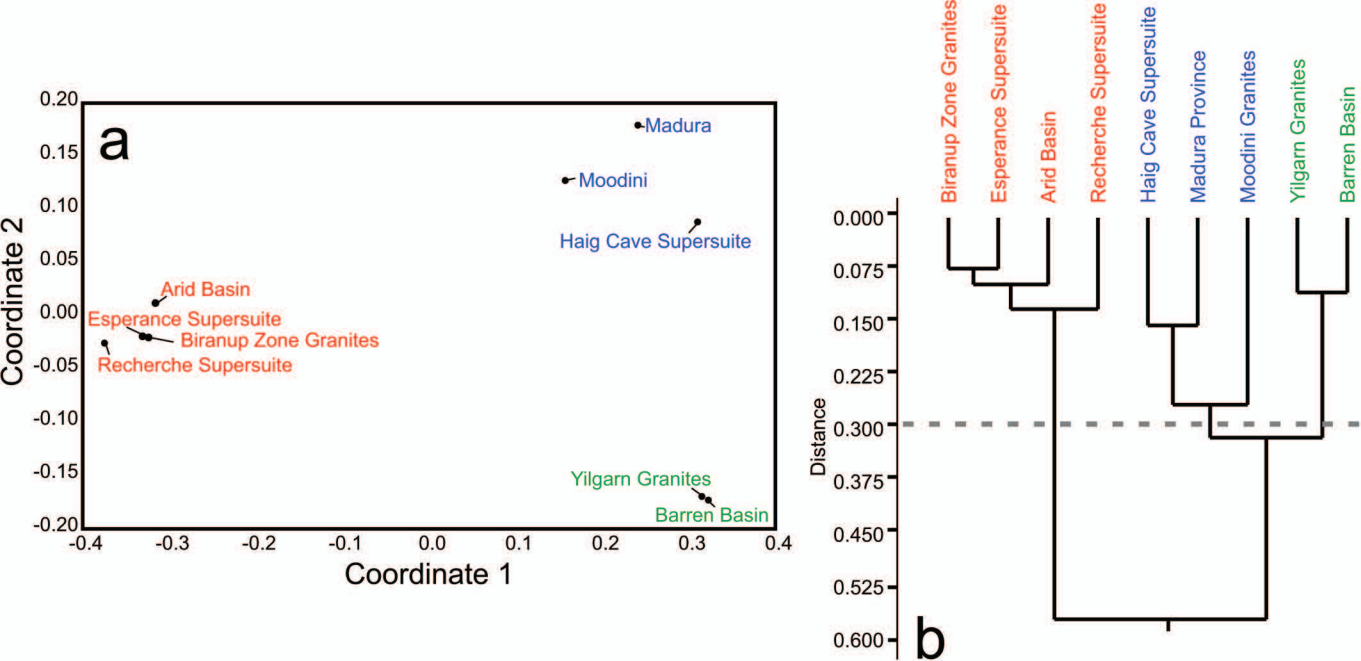
a
Madura
Moodini
Haig Cave Supersuite
Arid Basin
Esperance Supersuite
Biranup Zone Granites
Recherche Supersuite
Yilgarn Granites
Barren Basin
Coordinate 1
Coordinate 2
0.20
0.15
0.10
0.05
0.00
-0.05
-0.10
-0.15
-0.20
-0.4
-0.3
-0.2
-0.1
0.0
0.1
0.2
0.3
0.4
b
Biranup Zone Granites
Esperance Supersuite
Arid Basin
Recherche Supersuite
Haig Cave Supersuite
Madura Province
Moodini Granites
Yilgarn Granites
Barren Basin
Distance
0.000
0.075
0.150
0.225
0.300
0.375
0.450
0.525
0.600

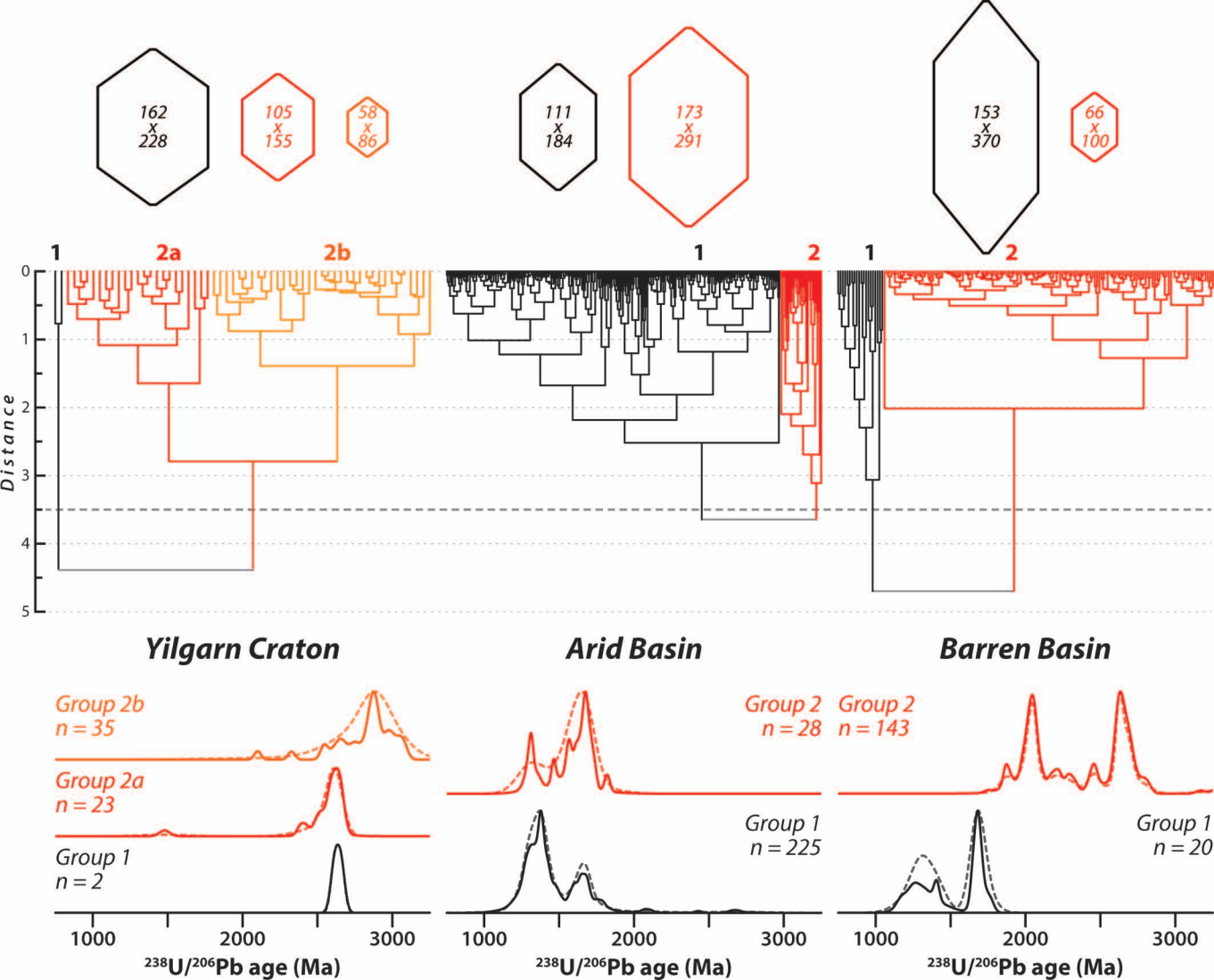
162
x
228
105
x
155
58
x
86
111
x
184
173
x
291
153
x
370
66
x
100
1
2a
2b
1
2
1
2
Distance
0
1
2
3
4
5
Yilgarn Craton
Arid Basin
Barren Basin
Group 2b
n = 35
Group 2a
n = 23
Group 1
n = 2
Group 2
n = 28
Group 1
n = 225
Group 2
n = 143
Group 1
n = 20
1000
2000
3000
238U/206Pb age (Ma)
1000
2000
3000
238U/206Pb age (Ma)
1000
2000
3000
238U/206Pb age (Ma)

TABLE 1 Definitions of shape descriptors used in this work. Equations after Russ (2011)

Effective diameter	Aspect ratio	Circularity	Roundness	Compactness	Area	Perimeter	Major axis	Minor axis
$2\times\sqrt{\frac{Area}{\pi}}$	$\frac{major\ axis}{minor\ axis}$	$\frac{4\pi\ x\ Area}{perimeter^2}$	$\frac{4\ Area}{\pi\ x\ (major\ axis)^2}$	$\frac{\sqrt{\frac{4\ area}{\pi}}}{major\ axis}$			*Measured in μm*	

TABLE 2 Summary of statistical values of grain shape measurements

Madura Shelf n = 231	Area	Perimeter (μm)	Major axis (μm)	Minor axis (μm)	Aspect ratio	Circularity	Compactness	Roundness	Effective Diameter (μm)
Min	2878.0	196.0	62.0	38.0	1.051	0.198	0.413	0.170	60.6
Max	40956.0	1613.0	374.0	180.0	5.844	0.941	0.977	0.954	228.4
Mean	10100.8	455.6	166.8	74.9	2.347	0.624	0.677	0.470	110.5
Standard deviation	5115.1	167.8	46.4	22.7	0.755	0.128	0.106	0.149	25.9
Median	8922.0	417.0	159.0	70.0	2.261	0.649	0.667	0.445	106.6
25 percentile	6722.0	355.0	134.0	61.0	1.800	0.561	0.601	0.361	92.5
75 percentile	11989.0	500.0	194.0	86.0	2.783	0.713	0.744	0.554	123.6
Skewness	2.0	2.9	1.1	1.5	1.168	−0.843	0.408	0.804	1.0
Kurtosis	7.0	13.3	2.1	3.6	3.008	1.077	−0.044	0.412	2.0
Esperance Supersuite n = 64	**Area**	**Perimeter (μm)**	**Major axis (μm)**	**Minor axis (μm)**	**Aspect ratio**	**Circularity**	**Compactness**	**Roundness**	**Effective Diameter (μm)**
Min	4658.0	271.0	88.0	55.0	1.255	0.543	0.539	0.291	77.0
Max	38218.0	805.0	353.0	198.0	3.446	0.859	0.893	0.797	220.6
Mean	19082.5	573.8	215.0	112.2	1.973	0.703	0.727	0.538	152.0
Standard deviation	8184.8	140.5	63.1	31.0	0.583	0.080	0.100	0.144	34.9
Median	18958.5	594.0	217.5	107.0	1.843	0.718	0.729	0.531	155.4
25 percentile	12611.5	467.0	163.5	87.3	1.553	0.643	0.642	0.412	126.7
75 percentile	25744.3	679.5	263.3	129.8	2.330	0.759	0.801	0.642	181.1
Skewness	0.2	−0.3	0.1	0.7	0.903	−0.155	−0.114	0.090	−0.2
Kurtosis	−0.6	−0.7	−0.7	0.3	−0.013	−0.754	−0.991	−1.002	−0.6
Recherche Supersuite n = 85	**Area**	**Perimeter (μm)**	**Major axis (μm)**	**Minor axis (μm)**	**Aspect ratio**	**Circularity**	**compactness**	**Roundness**	**Effective Diameter (μm)**
Min	5134.0	307.0	90.0	73.0	1.154	0.454	0.519	0.269	80.9
Max	37324.0	844.0	381.0	156.0	3.699	0.855	1.003	1.006	218.1
Mean	18054.7	561.8	210.3	114.1	1.857	0.705	0.722	0.529	149.6
Standard deviation	5967.7	99.7	45.2	16.4	0.396	0.065	0.084	0.126	25.0
Median	17343.0	548.0	206.0	112.0	1.798	0.709	0.707	0.500	148.6
25 percentile	13591.5	481.0	178.5	104.0	1.579	0.678	0.670	0.448	131.6
75 percentile	21284.0	625.0	239.0	125.0	2.060	0.743	0.761	0.580	164.7
Skewness	0.6	0.3	0.6	0.3	1.422	−0.819	0.565	1.021	0.1
Kurtosis	0.5	0.2	1.9	0.1	4.706	2.269	1.118	2.010	0.1
Haig Cave Supersuite n = 87	**Area**	**Perimeter (μm)**	**Major axis (μm)**	**Minor axis (μm)**	**Aspect ratio**	**Circularity**	**Compactness**	**Roundness**	**Effective Diameter (μm)**
Min	1863.0	194.0	103.0	78.0	1.061	0.325	0.495	0.245	48.7
Max	44263.0	989.0	336.0	240.0	1.861	0.987	1.892	3.578	237.5
Mean	9987.1	407.8	151.5	112.1	1.345	0.730	0.771	0.622	106.7
Standard deviation	7738.2	142.8	46.9	30.1	0.123	0.123	0.168	0.365	36.7
Median	7586.0	383.0	137.0	104.0	1.330	0.756	0.756	0.571	98.3
25 percentile	5162.0	315.0	120.0	92.0	1.264	0.671	0.670	0.450	81.1
75 percentile	10632.0	435.0	168.0	117.0	1.426	0.820	0.845	0.714	116.4
Skewness	2.3	1.7	1.9	2.0	0.757	−0.980	3.426	6.276	1.4
Kurtosis	6.3	3.4	4.1	4.1	2.698	1.213	22.406	50.651	2.2
Biranup Zone n = 96	**Area**	**Perimeter (μm)**	**Major axis (μm)**	**Minor axis (μm)**	**Aspect ratio**	**Circularity**	**Compactness**	**Roundness**	**Effective Diameter (μm)**
Min	4598.0	289.0	103.0	52.0	1.165	0.273	0.483	0.233	76.5
Max	73556.0	1290.0	393.0	216.0	3.431	0.853	1.274	1.624	306.1
Mean	22338.2	676.2	217.9	120.4	1.906	0.603	0.753	0.583	162.3
Standard deviation	12890.5	225.9	58.4	40.1	0.475	0.141	0.128	0.206	46.1
Median	19754.5	648.5	212.0	125.0	1.781	0.605	0.750	0.562	158.6
25 percentile	12616.5	490.0	180.5	84.5	1.552	0.498	0.662	0.439	126.8
75 percentile	28225.8	814.3	251.8	147.8	2.165	0.722	0.833	0.694	189.6

(Continues)

TABLE 2 (Continued)

Biranup Zone *n* = 96	Area	Perimeter (μm)	Major axis (μm)	Minor axis (μm)	Aspect ratio	Circularity	Compactness	Roundness	Effective Diameter (μm)
Skewness	1.3	0.6	0.4	0.1	0.878	−0.049	0.750	1.627	0.6
Kurtosis	2.3	−0.1	0.2	−0.9	0.369	−0.831	2.006	5.979	0.3
Yilgarn Craton *n* = 60	**Area**	**Perimeter (μm)**	**Major axis (μm)**	**Minor axis (μm)**	**Aspect ratio**	**Circularity**	**Compactness**	**Roundness**	**Effective Diameter (μm)**
Min	1256.0	143.0	49.0	32.0	1.217	0.480	0.537	0.289	40.0
Max	16945.0	586.0	240.0	163.0	2.083	0.953	0.980	0.961	146.9
Mean	6076.8	308.6	117.4	79.2	1.505	0.730	0.723	0.532	83.3
Standard deviation	4108.6	109.6	43.6	30.5	0.175	0.095	0.097	0.142	28.5
Median	5144.5	283.5	108.5	75.0	1.488	0.728	0.725	0.525	81.0
25 percentile	2565.0	205.3	78.0	49.0	1.366	0.670	0.654	0.428	57.2
75 percentile	8546.3	395.8	152.3	104.8	1.610	0.794	0.779	0.606	104.3
Skewness	1.0	0.7	0.7	0.5	0.744	0.062	0.049	0.430	0.5
Kurtosis	0.3	−0.3	−0.2	−0.1	0.793	0.356	−0.104	0.400	−0.7
Barren Basin *n* = 163	**Area**	**Perimeter (μm)**	**Major axis (μm)**	**Minor axis (μm)**	**Aspect ratio**	**Circularity**	**Compactness**	**Roundness**	**Effective Diameter (μm)**
Min	1056.0	131.0	45.0	21.0	1.011	0.456	0.474	0.225	36.7
Max	88024.0	1301.0	536.0	224.0	4.476	0.898	1.101	1.213	334.9
Mean	10287.5	363.6	133.3	76.3	1.730	0.778	0.788	0.633	99.9
Standard deviation	14526.5	230.8	96.4	36.3	0.588	0.089	0.109	0.169	56.1
Median	5304.0	289.0	104.0	68.0	1.604	0.803	0.795	0.633	82.2
25 percentile	4166.0	255.0	88.0	56.0	1.366	0.749	0.726	0.528	72.8
75 percentile	8108.0	353.0	124.0	87.0	1.897	0.840	0.860	0.740	101.6
Skewness	3.1	2.4	2.6	1.7	2.136	−1.586	−0.354	0.142	2.2
Kurtosis	10.1	5.2	6.5	3.7	5.916	2.537	0.507	0.455	4.6
Arid Basin *n* = 253	**Area**	**Perimeter (μm)**	**Major axis (μm)**	**Minor axis (μm)**	**Aspect ratio**	**Circularity**	**Compactness**	**Roundness**	**Effective Diameter (μm)**
Min	5056.0	274.0	90.0	52.0	0.863	0.427	0.457	0.209	80.3
Max	60272.0	1057.0	423.0	245.0	4.774	0.912	1.365	0.974	277.1
Mean	18761.6	542.3	195.9	118.2	1.728	0.771	0.793	0.642	150.1
Standard deviation	9572.4	149.8	65.8	31.3	0.650	0.105	0.129	0.190	37.0
Median	17191.0	521.0	183.0	116.0	1.512	0.800	0.809	0.661	148.0
25 percentile	11748.0	431.0	148.0	98.0	1.237	0.711	0.687	0.476	122.3
75 percentile	23317.5	619.5	229.0	135.0	2.081	0.850	0.896	0.803	172.3
Skewness	1.4	0.8	1.0	0.7	1.531	−1.119	−0.109	−0.239	0.7
Kurtosis	2.3	0.5	0.8	1.4	2.700	0.778	0.483	−1.015	0.4
Moodini Supersuite *n* = 20	**Area**	**Perimeter (μm)**	**Major axis (μm)**	**Minor axis (μm)**	**Aspect ratio**	**Circularity**	**Compactness**	**Roundness**	**Effective Diameter (μm)**
Min	5365.0	321.0	106.0	52.0	1.447	0.305	0.542	0.294	82.7
Max	16659.0	761.0	267.0	117.0	3.466	0.791	1.328	1.764	144.8
Mean	12165.3	512.0	178.0	78.1	2.363	0.595	0.721	0.554	118.6
Standard deviation	3543.9	111.6	40.5	17.5	0.675	0.116	0.191	0.349	15.1
Median	12423.5	510.0	186.5	72.0	2.194	0.596	0.692	0.479	123.4
25 percentile	9160.8	424.0	142.3	67.0	1.834	0.535	0.591	0.350	108.0
75 percentile	16156.5	585.3	204.0	93.5	3.049	0.685	0.741	0.548	129.1
Skewness	−0.3	0.3	−0.2	0.5	0.307	−0.546	2.169	2.711	−0.8
Kurtosis	−1.1	0.0	0.1	−0.4	−1.285	0.732	5.197	7.851	0.4

TABLE 3 Correlation test of grain shape and uranium and thorium concentrations [Colour table can be viewed at wileyonlinelibrary.com]

ESPERANCE	Major	Minor	ED	^{238}U (ppm)	^{232}Th (ppm)
Major		8.88E-05	6.55E-20	0.080202	0.36589
Minor	0.4701		5.53E-15	0.059294	0.3303
ED	0.86151	0.79325		0.035711	0.25498
^{238}U (ppm)	−0.22034	−0.23705	−0.26307		9.62E-07
^{232}Th (ppm)	−0.11491	−0.12366	−0.14439	0.56839	
RECHERCHE	**Major**	**Minor**	**ED**	**^{238}U (ppm)**	**^{232}Th (ppm)**
Major		0.00011573	2.82E-24	0.053044	0.089569
Minor	0.40599		3.27E-08	0.34846	0.90444
ED	0.84499	0.55617		0.85852	0.43077
^{238}U (ppm)	−0.21059	−0.10295	0.019624		1.22E-09
^{232}Th (ppm)	−0.18528	−0.013216	−0.086578	0.60066	
HAIG CAVE	**Major**	**Minor**	**ED**	**^{238}U (ppm)**	**^{232}Th (ppm)**
Major		8.67E-47	1.12E-19	0.40476	0.38479
Minor	0.95538		1.26E-21	0.18532	0.1397
ED	0.78905	0.81253		0.11931	0.18228
^{238}U (ppm)	0.090448	0.14335	0.16824		2.84E-24
^{232}Th (ppm)	0.094334	0.15963	0.14433	0.83987	
BIRANUP	**Major**	**Minor**	**ED**	**^{238}U (ppm)**	**^{232}Th (ppm)**
Major		4.53E-18	2.31E-25	0.0040242	0.22814
Minor	0.74287		3.05E-34	1.23E-05	0.26437
ED	0.82813	0.89236		5.59E-05	0.28644
^{238}U (ppm)	−0.29099	−0.43003	−0.39927		6.88E-15
^{232}Th (ppm)	−0.12415	−0.11504	−0.1099	0.69069	
YILGARN	**Major**	**Minor**	**ED**	**^{238}U (ppm)**	**^{232}Th (ppm)**
Major		2.74E-34	1.09E-25	2.91E-14	2.49E-05
Minor	0.96169		4.46E-23	5.23E-15	3.27E-05
ED	0.92273	0.90406		1.74E-13	0.00017141
^{238}U (ppm)	−0.79608	−0.80906	−0.78143		1.32E-09
^{232}Th (ppm)	−0.51562	−0.5091	−0.4666	0.68732	
ARID BASIN	**Major**	**Minor**	**ED**	**^{238}U (ppm)**	**^{232}Th (ppm)**
Major		1.08E-09	5.04E-64	0.75184	0.020858
Minor	0.37135		7.18E-50	0.69616	0.58663
ED	0.82454	0.76498		0.74466	0.32159
^{238}U (ppm)	−0.019977	0.024669	0.020576		1.55E-39
^{232}Th (ppm)	−0.14521	0.034343	−0.062564	0.70633	
BARREN BASIN	**Major**	**Minor**	**ED**	**^{238}U (ppm)**	**^{232}Th (ppm)**
Major		1.08E-09	5.04E-64	0.75184	0.020858
Minor	0.37135		7.18E-50	0.69616	0.58663
ED	0.82454	0.76498		0.74466	0.32159
^{238}U (ppm)	−0.019977	0.024669	0.020576		1.55E-39
^{232}Th (ppm)	−0.14521	0.034343	−0.062564	0.70633	

Correlation tests performed in PAST (Hammer et al., 2001). ED denotes Effective Diameter. Pearson correlation values are given in the bottom left of each matrix, with negative correlations in black text and positive correlations in grey text. Probability values assessing the data correlation are given in the upper right of each matrix with cells colour coded according to the strength of probability of correlation. Green cells for $p < .05$, yellow cells for $.05 < p < .10$, grey cells for $.10 < p < .5$, red cells for $p > .5$, indicating progressively weaker likelihood of any correlation.

TABLE 4 Summary F-test and *t*-test data for Arid and Barren Basin samples tested against regional crystalline source regions. [Colour table can be viewed at wileyonlinelibrary.com]

F-Test: Arid and Barren Basins versus crystalline sources

Arid	Yilgarn	Recherche	Haig	Esperance	Biranup
Major					
Minor					
Eff. D					
Barren	**Yilgarn**	**Recherche**	**Haig**	**Esperance**	**Biranup**
Major					
Minor					
Eff. D					

***t*-Test: Arid and Barren Basins versus crystalline sources**

Arid	Yilgarn	Recherche	Haig	Esperance	Biranup
Major	.0000	.0254	.0000	.0375	.0042
Minor	.0000	.1292	.1141	.1695	.5782
Eff. D	.0000	.8875	.0000	.7107	.0108
Barren	**Yilgarn**	**Recherche**	**Haig**	**Esperance**	**Biranup**
Major	.0934	.0000	.0458	.0000	.0000
Minor	.5829	.0000	.0000	.0000	.0000
Eff. D	.0042	.0000	.2471	.0000	.0000

Note. F-test cells with a red fill indicate rejection of the null hypothesis (alpha = 0.05), indicating statistical difference between the variances of the populations tested. F-test cells coloured in green indicate acceptance of the null hypothesis (alpha = 0.05) and a statistical inability to separate the two populations based on differences in variance values. The *t*-test cells are coloured similarly while testing population means rather than variance. Results of *t*-test also include an additional yellow class representing populations that are differentiated at an alpha value of 0.05, but not at 0.01. The *p* values of the *t*-test are also provided.

TABLE 5 Summary F-test and *t*-test data for Madura Shelf (Madura Formation) samples tested against regional crystalline source regions. [Colour table can be viewed at wileyonlinelibrary.com]

F-Test: Madura Shelf sediments versus crystalline sources

Madura Shelf	Yilgarn	Recherche	Haig	Esperance	Biranup	Moodini
Major						
Minor						
Eff. D						

***t*-Test: Madura Shelf sediments versus crystalline sources**

Madura Shelf	Yilgarn	Recherche	Haig	Esperance	Biranup	Moodini
Major	.0000	.0000	.0101	.0000	.0000	.3000
Minor	.2247	.0000	.0000	.0000	.0000	.5480
Eff. D	.0000	.0000	.3128	.0000	.0000	.0395

Note. F-test cells with a red fill indicate rejection of the null hypothesis (alpha = 0.05), indicating statistical difference between the variances of the populations tested. F-test cells coloured in green indicate acceptance of the null hypothesis (alpha = 0.05) and a statistical inability to separate the two populations based on differences in variance values. The *t*-test cells are coloured similarly while testing population means rather than variance. Results of *t*-test also include an additional yellow class representing populations that are differentiated at an alpha value of 0.05 but not at 0.01. The *p* values of the *t*-test are also provided.

TABLE 6 Kolmogorov–Smirnov D value matrix for zircon grain effective diameter [Colour table can be viewed at wileyonlinelibrary.com]

	Esperance Supersuite	Recherche Supersuite	Haig Cave Supersuite	Biranup Zone Granites	Yilgarn Granites	Arid Basin	Barren Basin	Madura Shelf	Moodini Supersuite
Esperance Supersuite	0	0.183	0.614	0.130	0.744	0.132	0.694	0.559	0.653
Recherche Supersuite	0.183	0	0.676	0.232	0.806	0.143	0.799	0.640	0.632
Haig Cave Supersuite	0.614	0.676	0	0.562	0.398	0.579	0.276	0.222	0.459
Biranup Zone Granites	0.130	0.232	0.562	0	0.733	0.164	0.720	0.588	0.669
Yilgarn Granites	0.744	0.806	0.398	0.733	0	0.726	0.254	0.449	0.617
Arid Basin	0.132	0.143	0.579	0.164	0.726	0	0.715	0.497	0.559
Barren Basin	0.694	0.799	0.276	0.720	0.254	0.715	0	0.447	0.636
Madura Shelf	0.559	0.640	0.222	0.588	0.449	0.497	0.447	0	0.354
Moodini Supersuite	0.653	0.632	0.459	0.669	0.617	0.559	0.636	0.354	0